J. Fluid Mech. (2007), *vol.* 577, *pp.* 251–273.
doi:10.1017/S0022112007004703 Printed in the United Kingdom

Mechanics of merging events for a series of layers in a stratified turbulent fluid

TIMOUR RADKO

Department of Oceanography, Naval Postgraduate School, Monterey, CA 93943, USA
tradko@nps.edu

(Received 8 February 2006 and in revised form 25 October 2006)

This study attempts to explain the evolutionary pattern of a series of well-mixed layers separated by thin high-gradient interfaces frequently observed in stratified fluids. Such layered structures form as a result of the instability of the equilibrium with uniform stratification, and their subsequent evolution is characterized by a sequence of merging events which systematically increase the average layer thickness. The coarsening of layers can take one of two forms, depending on the realized vertical buoyancy flux law. Layers merge either when the high-gradient interfaces drift and collide, or when some interfaces gradually erode without moving vertically. The selection of a preferred pattern of coarsening is rationalized by the analytical theory – the merging theorem – which is based on linear stability analysis for a series of identical layers and strongly stratified interfaces. The merging theorem suggests that the merger by erosion of weak interfaces occurs when the vertical buoyancy flux decreases with the buoyancy variation across the step. If the buoyancy flux increases with step height, then coarsening of a staircase may result from drift and collision of the adjacent interfaces. Our model also quantifies the time scale of merging events and makes it possible to predict whether the layer merging continues indefinitely or whether the coarsening is ultimately arrested. The merging theorem is applied to extant one-dimensional models of turbulent mixing and successfully tested against the corresponding fully nonlinear numerical simulations. It is hypothesized that the upscale cascade of buoyancy variance associated with merging events may be one of the significant sources of the fine-scale ($\sim$10 m) variability in the ocean.

1. Introduction

Small-scale turbulence in stratified fluids frequently results in the formation of a series of well-mixed layers separated by thin high gradient interfaces, which, in the oceanographic context, are commonly referred to as 'staircases'. Persistent stepped structures in the vertical temperature and salinity profiles have been well documented in the Tyrrhenian Sea, below the Mediterranean outflow, in the tropical Atlantic, and in the Arctic Ocean (see the reviews of Schmitt 1994, 2003; Kelley *et al.* 2003). While the generation of oceanic staircases is generally attributed to double-diffusive convection – an instability caused by the difference in the molecular diffusivities of the individual density components – the staircases have been observed occasionally even when the stratification is double-diffusively stable. Examples of such staircases include observations of the stepwise temperature profiles in fresh-water lakes (Simpson & Woods 1970) and laboratory experiments with turbulent one-component flows (Ruddick, McDougall & Turner 1989; Park, Whitehead & Gnanadeskian 1994;

Holford & Linden 1999). Regardless of whether the staircases are produced by double-diffusion or by the mechanically generated turbulence, their formation can be related to instabilities of the vertical buoyancy flux laws (Phillips 1972; Posmentier 1977; Balmforth, Llewellyn Smith & Young 1998). These studies discuss the evolution of staircases in terms of the solutions of the buoyancy conservation equation

$$\frac{\partial b}{\partial t} = \frac{\partial F}{\partial z}, \tag{1}$$

where $b(z, t)$ is the buoyancy and $F(z, t)$ is the downward buoyancy flux, which is assumed to be controlled by the buoyancy distribution. The buoyancy flux does not necessarily instantaneously adjust to the buoyancy profile and can retain some fading memory of the buoyancy distribution in the past. To explain the origin of staircases, several studies formulated heuristic one-dimensional models of the buoyancy flux F (Balmforth *et al.* 1998; Radko 2003). They demonstrated that the uniform large-scale buoyancy gradient ($b_z = const$), a trivial solution of (1) with uniform flux F, can be unstable. This instability manifests itself in the form of growing, horizontally uniform perturbations, which eventually transform the vertical buoyancy profile into a well-defined staircase.

Before going on to discuss the staircases in stratified turbulent fluids, it should be noted that the processes under consideration have direct counterparts in many other physical systems. Natural sciences often deal with conserved quantities whose dynamics are governed by the conservation law (1), where b and z do not necessarily represent the buoyancy and the vertical coordinate. Examples of such systems include the theory of phase transitions (Cahn & Hilliard 1958; Bates & Xun 1995); similar problems arise in meteorology (Manfroi & Young 1999), traffic flow theory (Whitham 1974), and engineering (Chapman & Proctor 1980). The instabilities of various flux laws are common, and the resulting stepped solutions have been extensively studied. Development of strong jets in the homogeneous beta-plane turbulence (Rhines 1975), the upscale energy transfer in baroclinically unstable flows (Panetta 1993), and the Kolmogorov flow (Meshalkin & Sinai 1961; Balmforth & Young 2002) – these and many other problems can be phrased in terms of the instability of one-dimensional conservation equations. The specifics of each system are reflected in the expressions for F in (1), the flux law models, which are dictated by the relevant physics and dynamics at play. To be precise, this paper is focused on the oceanographic application of our theory – the generation and evolution of steps in the vertical buoyancy profile, although the proposed framework is believed to be of much broader fluid dynamical relevance. Consequently, we shall continue to refer to b, z and F as the buoyancy, vertical coordinate and buoyancy flux, respectively.

A ubiquitous feature of staircases in stratified fluids is related to their evolution in time. Field observations (Zodiatis & Gasparini 1996), theoretical models (Balmforth *et al.* 1998), laboratory (Park *et al.* 1994) and numerical (Radko 2003) experiments, all indicate that the layers which develop initially are unsteady. The layers formed first are relatively thin. However, in time, they merge continuously and the characteristic step height increases correspondingly. The evolution of a series of pronounced layers has been attributed – see the discussion in Huppert (1971) and Radko (2005) in the context of oceanic double-diffusion – to the secondary instabilities of steady-state staircases. Laboratory experiments indicate that the coarsening of staircases takes one of two forms; layers merge either when interfaces drift and collide, or when interfaces gradually erode without moving vertically (e.g. Park *et al.* 1994). Both forms of coarsening were reproduced by the numerical simulations of the

one-dimensional parameterized equations. Thus, Balmforth *et al.* (1998) used the 'mixing length' argument to construct a model of the mechanically forced turbulence in a stratified fluid which expresses the vertical buoyancy flux in terms of the local buoyancy gradient and the density of the kinetic energy. Integration of their model equations indicated that the preferred mechanism of coarsening is associated with the vertical drift and collision of interfaces, a process which will be referred to as H-merger. On the other hand, Merryfield (2000) modelled the upgradient buoyancy flux in a double-diffusive fluid and noticed a tendency for the steps with small buoyancy variation to weaken even more and ultimately disappear – the 'B-merger' in our notation. Although these experiments indicate that the evolution of layers in one-dimensional models is sensitive to the buoyancy flux law, the selection of the preferred pattern of coarsening has not been properly explained yet.

This paper attempts to formulate a framework for discussion of merging events which is based on linear stability analysis for a series of identical steps. It is argued that the observed merging events are directly linked to the two modes of instability. In the first mode (B-instability), slightly stronger – in terms of buoyancy variation – interfaces grow further at the expense of weaker interfaces. In the second mode (H-instability), slightly thicker layers thicken even more while thin layers shrink and ultimately disappear. The key result of the stability analysis is expressed by the 'merging theorem', which states that if the buoyancy flux decreases with the buoyancy variation across the step, then the staircase is affected by the B-instability, and the spontaneous merger of layers occurs through gradual erosion of weak interfaces. If, however, fluxes increase with step height, then coarsening of a staircase may result from drift and collision of the adjacent interfaces. If both conditions are satisfied, the preferred mechanism of coarsening is determined by the unstable mode with the largest growth rate. These findings are used to rationalize the behaviour of staircases noted in the aforementioned laboratory and numerical studies.

The merging theorem naturally leads to a simple technique for predicting, for any given mixing model, the preferred pattern of coarsening, time scale of merging events, and the ultimate fate of staircases. In connection with the latter issue, it should be mentioned that Balmforth *et al.* and Merryfield's numerical calculations suggest that merging events go on indefinitely and therefore the step thickness inevitably increases to the largest resolved scale of the experiment. While the endless coarsening, as we demonstrate here, is possible for certain flux laws, there is no reason to expect that it is the only, or even the most likely, scenario for the evolution of staircases in time. Thus, Radko (2005) gives an example of the double-diffusive staircase which eventually evolves to a fully equilibrated state. The mergers in his model cease when the average layer thickness reaches a critical value, greatly exceeding the initial step height.

This paper is set out as follows. In § 2, we perform a linear stability analysis for a series of identical steps and use it to formulate general criteria for the H- and B-type merging events. In § 3 we revisit the one-dimensional models of vertical mixing formulated by Balmforth *et al.* (1998) and Merryfield (2000), focusing our inquiry on the dynamics of coarsening in simulated staircases. In § 4, we test the merging theorem by applying it to the models in § 3 and comparing its predictions with the corresponding numerical results. We summarize and draw conclusions in § 5.

2. The merging theorem

Our starting point is the stepped solution of the one-dimensional buoyancy conservation equation (1), and the following analysis attempts to establish the basic

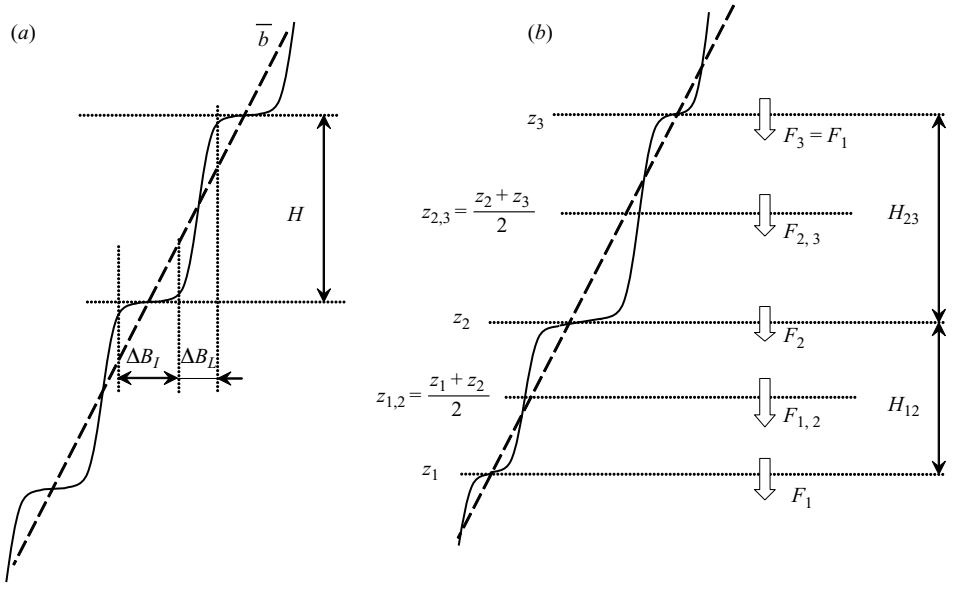

FIGURE 1. Schematic diagram illustrating the stability analysis for an infinite series of layers and interfaces. (*a*) Basic state consisting of identical steps. (*b*) Perturbed state in which the buoyancy jumps at even interfaces are slightly increased and the jumps at odd interfaces are decreased correspondingly. The interfaces are displaced vertically, and therefore thicknesses of the adjacent layers are different.

principles of its evolution in time. The particular form of the flux law F is unspecified at this point. We assume, however, that this flux law is such that the solution with uniform buoyancy gradient is unstable, and the result of this instability is a series of relatively well-mixed layers separated by thin high-gradient interfaces – a staircase. To gain a preliminary understanding of the interaction between layers in the staircase, we consider the dynamics of a simple, yet illuminating system (figure 1). The schematic diagram in figure 1(*a*) shows a basic state consisting of a series of identical thin high-gradient interfaces separated by low-gradient layers of equal thickness H. The thickness of the high-gradient interfaces is assumed to be negligible compared to the thickness of the layers. Following Radko (2005), we perturb this steady state as indicated in figure 1(*b*). The jump in buoyancy across the interface at $z = z_2$ is slightly increased, which is compensated by decrease in the strength of the interfaces at $z = z_1$ and $z = z_3$; $b_{n\,n+1}$ denotes the value of buoyancy at the level exactly between two adjacent interfaces $z_{n\,n+1} = (z_n + z_{n+1})/2$. The buoyancy variations across the two steps in figure 1(*b*) are expressed as follows:

$$\left.\begin{aligned} b_{12} - b_{01} &= B - \delta \\ b_{23} - b_{12} &= B + \delta \end{aligned}\right\} \quad \delta \ll B, \tag{2}$$

where $B = (\partial \bar{b}/\partial z)H$ is the buoyancy variation over one step in the undisturbed staircase in figure 1(*a*) and δ is a small perturbation. The thicknesses of the adjacent layers in figure 1(*b*) are not necessarily equal:

$$\left.\begin{aligned} H_{12} &= H - h \\ H_{23} &= H + h \end{aligned}\right\} \quad h \ll H, \tag{3}$$

where $H_{n\,n+1}$ is the distance between the interfaces at $z = z_n$ and $z = z_{n+1}$. The system of layers and interfaces in figure 1(*b*) is periodic with the z-wavelength of $2H$, and perturbing the basic state in such a manner does not affect the overall buoyancy gradient. Our objective is to determine whether the disturbance will grow in time, implying instability of the basic state in figure 1(*a*), or remain small. The essential difference between this model and that studied in Radko (2005) is that the high-gradient interfaces are allowed to drift vertically.

For our purpose, it is convenient to use the buoyancy equation in the integral form, which is obtained by integrating (1) over an arbitrary interval $[z_{bot}, z_{top}]$:

$$\int_{z_{bot}}^{z_{top}} \frac{\partial b}{\partial t}\,\mathrm{d}z = \int_{z_{bot}}^{z_{top}} \frac{\partial F}{\partial z}\,\mathrm{d}z = F(z_{top}) - F(z_{bot}), \tag{4}$$

where $z_{top}(t)$ and $z_{bot}(t)$ are two levels which may vary in time. Using the identity

$$\frac{\mathrm{d}}{\mathrm{d}t}\int_{z_{bot}}^{z_{top}} b\,\mathrm{d}z = \int_{z_{bot}}^{z_{top}} \frac{\partial b}{\partial t}\,\mathrm{d}z + \frac{\mathrm{d}z_{top}}{\mathrm{d}t}b(z_{top}) - \frac{\mathrm{d}z_{bot}}{\mathrm{d}t}b(z_{bot}), \tag{5}$$

we rewrite (4) as

$$\frac{\mathrm{d}}{\mathrm{d}t}\int_{z_{bot}}^{z_{top}} b\,\mathrm{d}z = \frac{\mathrm{d}z_{top}}{\mathrm{d}t}b(z_{top}) - \frac{\mathrm{d}z_{bot}}{\mathrm{d}t}b(z_{bot}) + F(z_{top}) - F(z_{bot}). \tag{6}$$

The integral relation (6) is first applied to the individual layers $[z_n, z_{n+1}]$:

$$\frac{\mathrm{d}}{\mathrm{d}t}\int_{z_n}^{z_{n+1}} b\,\mathrm{d}z = \frac{\mathrm{d}z_{n+1}}{\mathrm{d}t}b_{n+1} - \frac{\mathrm{d}z_n}{\mathrm{d}t}b_n + F_{n+1} - F_n, \tag{7}$$

where $F_i = F(z_i)$. The major contribution to the integral of buoyancy in (7) comes from the interior part of layers where the buoyancy gradient is nearly uniform, and therefore

$$\int_{z_n}^{z_{n+1}} b\,\mathrm{d}z \approx b_{n\,n+1}H_{n\,n+1}. \tag{8}$$

Applying (7) and (8) to two consecutive layers $[z_n, z_{n+1}]$ where $n = 1, 2$ results in

$$\left.\begin{aligned}\frac{\mathrm{d}}{\mathrm{d}t}(H_{12}b_{12}) &= F_2 - F_1 + \frac{\mathrm{d}z_2}{\mathrm{d}t}b_2 - \frac{\mathrm{d}z_1}{\mathrm{d}t}b_1,\\ \frac{\mathrm{d}}{\mathrm{d}t}(H_{23}b_{23}) &= F_3 - F_2 + \frac{\mathrm{d}z_3}{\mathrm{d}t}b_3 - \frac{\mathrm{d}z_2}{\mathrm{d}t}b_2.\end{aligned}\right\} \tag{9}$$

Since there is a considerable variation in buoyancy across the high-gradient interfaces, it becomes necessary at this point to provide a precise definition of 'buoyancy at the interface' b_n in (9). Without loss of generality, we define the centre of the interface as a point where the buoyancy is an average of the values at the centres of the two adjacent layers:

$$b_n = \frac{b_{n-1\,n} + b_{n\,n+1}}{2}. \tag{10}$$

A similar set of integral relations results from the buoyancy budgets for regions bounded by the centres of the adjacent layers ($z_{n\,n+1}$):

$$\left.\begin{aligned}\frac{\mathrm{d}}{\mathrm{d}t}\left(\frac{H_{12}b_{12}}{2}+\frac{H_{23}b_{23}}{2}+\frac{H_{12}\Delta B_{L12}}{8}-\frac{H_{23}\Delta B_{L23}}{8}\right)&=\frac{\mathrm{d}z_{23}}{\mathrm{d}t}b_{23}-\frac{\mathrm{d}z_{12}}{\mathrm{d}t}b_{12}+F_{23}-F_{12},\\ \frac{\mathrm{d}}{\mathrm{d}t}\left(\frac{H_{23}b_{23}}{2}+\frac{H_{34}b_{34}}{2}+\frac{H_{23}\Delta B_{L23}}{8}-\frac{H_{34}\Delta B_{L34}}{8}\right)&=\frac{\mathrm{d}z_{34}}{\mathrm{d}t}b_{34}-\frac{\mathrm{d}z_{23}}{\mathrm{d}t}b_{23}+F_{34}-F_{23},\end{aligned}\right\}\tag{11}$$

where $F_{n\,n+1}=F(z_{n\,n+1})$; ΔB_{L12} and ΔB_{L23} are the buoyancy variations across the interior of the layers in figure 1(*b*). Next, we use (9) and (11) to formulate the equations for evolution of δ and h in time. For the δ-equation, we subtract the two equations in (9). This result is further simplified by using the periodicity conditions ($F_3=F_1$, $\mathrm{d}z_3/\mathrm{d}t=\mathrm{d}z_1/\mathrm{d}t$, $b_3=b_1+2B$) and (3):

$$\frac{\mathrm{d}}{\mathrm{d}t}[H(B+\delta)+h(b_{23}+b_{12})]=-2(F_2-F_1)+\frac{\mathrm{d}z_1}{\mathrm{d}t}(b_3+b_1)-2\frac{\mathrm{d}z_2}{\mathrm{d}t}b_2.\tag{12}$$

Equation (10), combined with the periodicity conditions $b_{01}=b_{23}-2B$ and $b_{34}=b_{12}+2B$, implies that

$$b_1+b_3=2b_2,$$

which further reduces (12) to

$$H\frac{\mathrm{d}\delta}{\mathrm{d}t}+2h\frac{\mathrm{d}b_2}{\mathrm{d}t}=-2(F_2-F_1).\tag{13}$$

This equation simplifies further when we consider perturbations that are weak relative to the basic state ($\delta\ll B$, $h\ll H$) and linearize (13) accordingly. Since $\mathrm{d}b_2/\mathrm{d}t=0$ in the basic steady state, this quantity is (at most) of the same order as the perturbation. Neglecting the nonlinear term $h(\mathrm{d}b_2/\mathrm{d}t)$ in (13) reduces our δ-equation to

$$\frac{\mathrm{d}}{\mathrm{d}t}\delta=-\frac{2}{H}(F_2-F_1).\tag{14}$$

Similarly, (11) is used to formulate an equation for h. The two equations in (11) are subtracted, the result is simplified using the periodicity conditions:

$$B\frac{\mathrm{d}h}{\mathrm{d}t}-\frac{\Delta B_{L12}+\Delta B_{L23}}{4}\frac{\mathrm{d}h}{\mathrm{d}t}-\frac{H}{4}\frac{\mathrm{d}}{\mathrm{d}t}(\Delta B_{L23}-\Delta B_{L12})=2(F_{23}-F_{12})+2\frac{\mathrm{d}z_{12}}{\mathrm{d}t}\delta,\tag{15}$$

and (15) is linearized about the steady state in figure 1(*a*). Since $\mathrm{d}z_{12}/\mathrm{d}t=0$ in the basic steady state, this quantity tends to zero in the limit of a weak perturbation, and therefore the nonlinear term $2(\mathrm{d}z_{12}/\mathrm{d}t)\delta$ in (15) is neglected. We also note that at leading order, $\Delta B_{L12}\approx\Delta B_{L23}\approx\Delta B_L$, which reduces the h-equation to

$$\left(B-\frac{\Delta B_L}{2}\right)\frac{\mathrm{d}h}{\mathrm{d}t}-\frac{H}{4}\frac{\mathrm{d}}{\mathrm{d}t}(\Delta B_{L23}-\Delta B_{L12})=2(F_{23}-F_{12}).\tag{16}$$

To solve the equations in (14) and (16), it becomes necessary to specify how the buoyancy fluxes at the interfaces and layers (F_n and $F_{n\,n+1}$) respond to changes in (δ, h). For that, we introduce a new quantity – the steady 'one-step' flux $\tilde{F}$. The one-step structure represents an elementary steady single-step solution of the governing equations for given step height $\tilde{H}$ and buoyancy variation $\tilde{B}$ [i.e. $b(\tilde{H})=b(0)+\tilde{B}$]; we also impose the periodic boundary conditions on the buoyancy gradient [$b_z(0)=b_z(\tilde{H})$] and its derivatives at $z=0$ and $z=\tilde{H}$. Consequently, the fluxes in the

one-step solution are determined by two quantities, the buoyancy variation across the step ($\tilde{B}$) and the step height ($\tilde{H}$). Some specific examples of the one-step flux laws $\tilde{F} = \tilde{F}(\tilde{B}, \tilde{H})$ are presented in Appendices A and B. (It is also possible to extend the merging theorem to the case when the one-step fluxes are determined by a larger number of variables. Here we present only the simplest version of the theory.) Next, the fluxes in (14) and (16) are approximated by the one-step laws. Note that replacing the instantaneous fluxes in the evolving staircase with the steady-state flux laws involves an implicit assumption that the time scale for adjustment of the one-step flux ($\tilde{F}$) to changes in step height and buoyancy variation is much less than the time scale of merging instability. This assumption, however, is likely to be satisfied and is generally easy to justify – in § 4 we consider specific mixing models and show that the one-step flux adjustment is indeed much faster than merging.

The instantaneous fluxes in layers and interfaces F_n and $F_{n\,n+1}$ in (14) and (16) are replaced by their steady-state counterparts as follows. Flux at the nth interface (F_n) is approximated by the one-step flux $\tilde{F}$ based on the parameters of a region extending between the centres of two adjacent layers ($z_{n-1\,n}$ and $z_{n\,n+1}$):

$$\left.\begin{aligned} F_1 &\approx \tilde{F}(b_{12} - b_{01}, z_{12} - z_{01}), \\ F_2 &\approx \tilde{F}(b_{23} - b_{12}, z_{23} - z_{12}). \end{aligned}\right\} \tag{17}$$

Since $z_{23} - z_{12} = z_{12} - z_{01} = H$, the difference between fluxes at the adjacent interfaces reduces, at leading order, to

$$F_2 - F_1 = \left.\frac{\partial \tilde{F}}{\partial \tilde{B}}\right|_{\substack{\tilde{H}=H \\ \tilde{B}=B}} 2\delta, \tag{18}$$

and (14) becomes

$$\frac{\mathrm{d}}{\mathrm{d}t}\delta = -\frac{4\delta}{H}\left.\frac{\partial \tilde{F}}{\partial \tilde{B}}\right|_{\substack{\tilde{H}=H \\ \tilde{B}=B}}. \tag{19}$$

Similarly, we assume and subsequently verify that the flux at the centre of each layer ($F_{n\,n+1}$) can be approximated by its one-step counterpart based on thickness and buoyancy variation across this layer

$$\left.\begin{aligned} F_{12} &= \tilde{F}(b_2 - b_1, z_2 - z_1), \\ F_{23} &= \tilde{F}(b_3 - b_2, z_3 - z_2). \end{aligned}\right\} \tag{20}$$

Since $b_3 - b_2 = b_2 - b_1 = B$, the h-equation in (16) reduces to

$$\left(B - \frac{\Delta B_L}{2}\right)\frac{\mathrm{d}h}{\mathrm{d}t} - \frac{H}{4}\frac{\mathrm{d}}{\mathrm{d}t}(\Delta B_{L23} - \Delta B_{L12}) = 4h\left.\frac{\partial \tilde{F}}{\partial \tilde{H}}\right|_{\substack{\tilde{H}=H \\ \tilde{B}=B}}. \tag{21}$$

The variation of the interior gradients in (21) is written as

$$\Delta B_{L23} - \Delta B_{L12} = \left.\frac{\partial \Delta B_L}{\partial \tilde{H}}\right|_{\substack{\tilde{H}=H \\ \tilde{B}=B}} 2h, \tag{22}$$

and substitution of the normal modes $(\delta, h) = (\delta_0, h_0)\exp(\lambda t)$ in (19) and (21) yields the eigenvalue equation for growth rates:

$$\lambda_B = -\frac{4}{H}\frac{\partial \tilde{F}}{\partial \tilde{B}}, \quad \lambda_H = \frac{4\dfrac{\partial \tilde{F}}{\partial \tilde{H}}}{B - \dfrac{\Delta B_L}{2} - \dfrac{H}{2}\dfrac{\partial \Delta B_L}{\partial \tilde{H}}}. \tag{23a, b}$$

We also note in passing that if the buoyancy variation over the high-gradient interfaces greatly exceeds its variation over layers (i.e. $\Delta B_L \ll B$), the equations for H-instability in (21) and (23) further reduce to

$$B\frac{\mathrm{d}h}{\mathrm{d}t} \approx 4h\frac{\partial \tilde{F}}{\partial \tilde{H}}, \quad \lambda_H \approx \frac{4}{B}\frac{\partial \tilde{F}}{\partial \tilde{H}}. \tag{24}$$

Equation (23) provides an insight into the selection of the staircase coarsening pattern. If the one-step buoyancy flux $\tilde{F}$ decreases with the buoyancy variation, then a series of identical steps is affected by the B-instability. The monotonic growth of δ in (2) has the effect of increasing the buoyancy variation across a step for which this variation is already large – at the expense of the weaker one. Thus, the spontaneous merger of layers in this case is expected to occur through gradual erosion of weak interfaces, as in Merryifield (2000). If, however, fluxes increase with step height, then h grows monotonically and coarsening of a staircase may result from the drift and collision of adjacent interfaces (as in Balmforth *et al.* 1998). If both conditions are satisfied, the preferred mechanism of coarsening depends on the relative magnitudes of the growth rates in (23).

The foregoing framework offers a simple technique for determining, for any given flux law, the evolutionary pattern of staircases. This technique can be summarized in three steps.

(i) Formulation of the steady state one-step flux laws $\tilde{F} = \tilde{F}(\tilde{B}, \tilde{H})$ – see Appendices A and B for examples of $\tilde{F}$ computed from the assumed flux-gradient relations (F).

(ii) Evaluation of the growth rates of the B- and H-instabilities using (23).

(iii) Prediction of the evolutionary pattern of layers and the ultimate fate of the staircase by focusing on the faster growing mode.

Of course, the possibility always exists that some mixing models may not satisfy the assumptions of the merging theorem. All the following examples, however, indicate that its predictions are remarkably accurate in describing the behaviour of simulated staircases. Likewise, we are aware of no flux model that would violate the conditions of the merging theorem.

3. Illustrative examples

In the following, the technique proposed in § 2 is applied to the specific flux models. While possible applications of the merging theorem are numerous – several have been mentioned in § 1, the choice of illustrative examples reflects the author's current interest in the dynamics of vertical mixing in stratified fluids.

3.1. *Mechanically forced stratified turbulence*

Our first example is a one-dimensional model formulated by Balmforth *et al.* (1998), which is meant to represent dynamics of a stratified turbulent fluid forced by a stirring

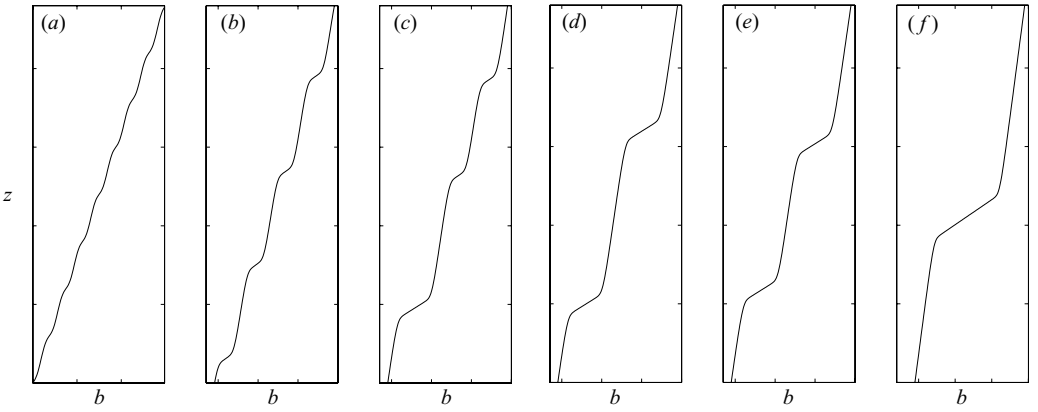

FIGURE 2. Formation and evolution of layers in the numerical experiment with Balmforth *et al.*'s model (25). The buoyancy profiles are shown at (*a–f*) $t = 6 \times 10^3$, 1.4×10^4, 1.4×10^5, 3×10^6, 7.6×10^6, 10^7. The appearance of well-defined layers in (*a*) is followed by a series of merging events in (*b–f*).

device:

$$\left.\begin{aligned} g_t &= \left(le^{1/2}g\right)_{zz}, & l &= \frac{e^{1/2}}{(e+g)^{1/2}}, \\ e_t &= \left(le^{1/2}e_z\right)_z - le^{1/2}g & &+ \frac{(1-e)e^{1/2}}{rl}. \end{aligned}\right\} \tag{25}$$

Here, $g = b_z$ is the buoyancy gradient and e is the kinetic energy density, non-dimensionalized using the speed and size of a stirring device (see Balmforth *et al.* 1998, for details); the value of the dimensionless constant r used in the subsequent calculations is $r = 50$. The vertical (downward) buoyancy flux in this model is

$$F = le^{1/2}g = \frac{eg}{(e+g)^{1/2}}. \tag{26}$$

Linear stability analysis in Balmforth *et al.* (1998) indicates that the uniform buoyancy gradient ($\bar{g}$) – a steady-state solution of (25) – is unstable for a finite range of $\bar{g}$:

$$g_{low} < \bar{g} < g_{high}, \tag{27}$$

where $g_{low} = 0.014$ and $g_{high} = 0.036$. The model equations (25) were rewritten with buoyancy (rather than z) as the independent variable and then integrated in time using a pseudospectral method analogous to that employed by Radko (2005). The periodic boundary conditions for (g, e) were imposed at the ends of the computational interval $z = 0, L_z$. Calculations were initialized by the uniform gradient $\bar{g} = 0.025$, slightly perturbed by a normal mode with wavelength $W = 30$. The chosen height of the computational domain was $L_z = 8W = 240$, resolved by $N = 128$ elements.

Figure 2 presents the evolution of the buoyancy profile $b(z)$. The first stage of this experiment is characterized by the growth of the unstable perturbation; modification of the initial buoyancy distribution at $t = 6 \times 10^3$ is shown in figure 2(*a*). By $t = 1.4 \times 10^4$ (figure 2*b*), the evolutionary pattern changes as high-gradient interfaces start to migrate vertically. Figures 2(*b*)–(*f*) illustrate the resulting coarsening of the staircase: layers are not steady, but undergo a series of binary mergers, which leaves only one layer within the limits of our computational domain at $t = 10^7$ in figure 2(*f*). Figure 3 plots the buoyancy gradient $b(z)$ as a function of time and z and reveals that

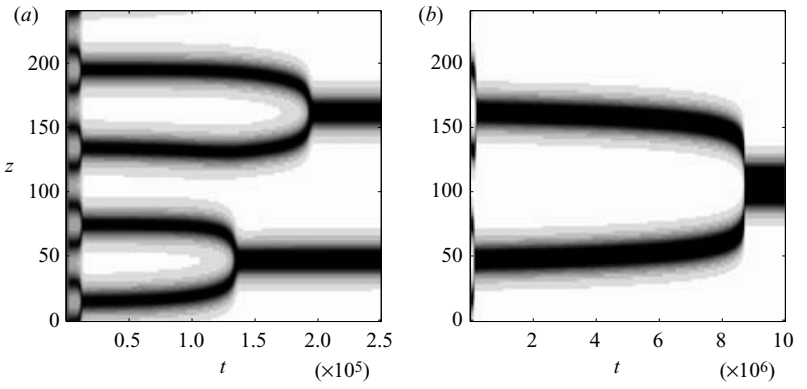

FIGURE 3. Space–time diagram of the buoyancy gradient for the experiment in figure 2. Dark colour represents high-gradient regions. (*a*) Long time resolution, (*b*) short time resolution. Note that the merger of steps is associated with the drift and collision of interfaces (the H-merger scenario).

the merger events are associated with the drift and collision of adjacent interfaces – the H-merger in our notation. The buoyancy jumps across the colliding interfaces remain nearly equal.

3.2. *Upgradient buoyancy flux*

Our second example – and probably the simplest layer-forming mixing model – represents the slow upgradient flux of density produced by double diffusion. This model was discussed by Merryfield (2000), who examined the numerical solutions of the piecewise-uniform linear diffusion equation

$$\left.\begin{aligned} \frac{\partial}{\partial t}b = K_f\frac{\partial^2 b}{\partial z^2},\ K_f<0 \text{ for } \frac{\partial b}{\partial z}>0 \\ \frac{\partial}{\partial t}b = K_c\frac{\partial^2 b}{\partial z^2},\ K_c>0 \text{ for } \frac{\partial b}{\partial z}<0 \end{aligned}\right\}\ K_c \gg |K_f|, \tag{28}$$

where b is the buoyancy, K_f is the diffusivity of buoyancy in the double-diffusive interfaces, and K_c is the diffusivity in the convecting layers. Double diffusion is driven by the release of the potential energy by one of the density components, and therefore it necessarily requires an overall potential energy decrease. Hence, the buoyancy flux is upward (i.e. counter gradient) and diffusivity in the double-diffusive interfaces (K_f) is negative. The interfaces are separated by turbulent convecting layers, whose dynamics are crudely modelled by strong downgradient diffusion (large positive K_c). While this model clearly oversimplifies the dynamics of the double diffusive staircases, it provides a convenient illustration of a coarsening pattern which is referred to here as the B-merger.

One of the mathematical difficulties with regard to (28) is that the diffusion equation with negative diffusivity is an ill-posed problem. Small-scale perturbations to the uniform gradient amplify most rapidly, and their growth rate diverges as the wavenumber increases. However, the ultraviolet catastrophe in this model is rather unphysical, since in a double-diffusive fluid there is a minimum amplified wavelength, whose scale is set by the nominal width of the salt fingers (the few centimetre filaments generated by the primary double-diffusive instability). In order to introduce this high-wavenumber cutoff in the model formulation, and thereby surmount the problem of

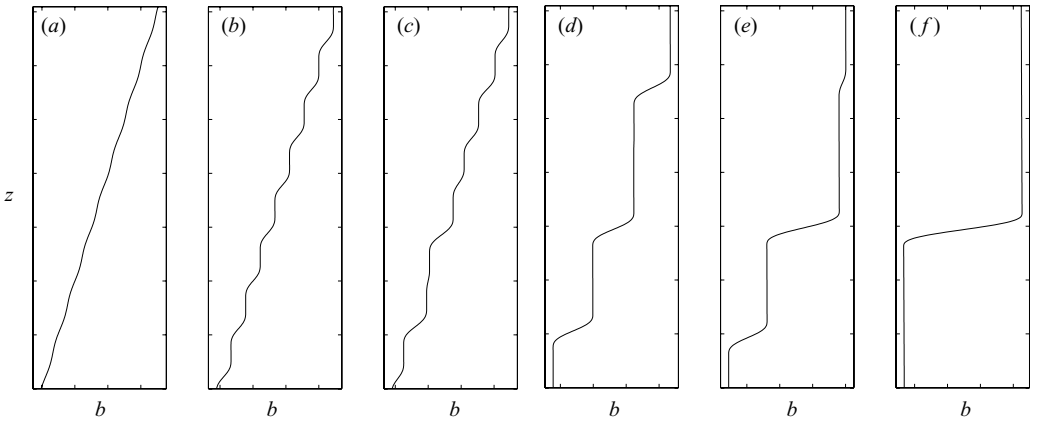

FIGURE 4. Formation and evolution of layers in the numerical experiment with the upgradient flux model, (29). The buoyancy profiles are shown at (*a–f*) $t = 5$, 20, 75, 120, 240, 400. Note the appearance of nearly homogeneous convecting layers separated by stratified interfaces at $t = 20$, followed by a series of merging events.

ill-posedness, the governing equations (28) are modified by adding the hyperdiffusion term $-\mu(\partial^4 b/\partial z^4)$. This modification suppresses the growth of small-scale modes, but has little effect on scales that significantly exceed the salt-finger width.

Following Radko (2005), we consider the buoyancy field consisting of the linear basic state $\bar{b}$, which remains unaltered in time, and a departure b' from it. Periodic conditions are assumed for b' at the ends of the interval $z = [0, L_z]$. The equations of motion are non-dimensionalized using $L = \sqrt{\mu/|K_f|}$ as a unit of length, $L^2/|K_f|$ as a unit of time, and $\bar{b}_z L$ as a unit of buoyancy. The buoyancy equation in non-dimensional units reduces to:

$$\frac{\partial b}{\partial t} = -\frac{\partial^2 b}{\partial z^2} - \frac{\partial^4 b}{\partial z^4} \qquad \text{for } \frac{\partial b}{\partial z} > 0, \tag{29a}$$

$$\frac{\partial b}{\partial t} = \frac{K_c}{|K_f|}\frac{\partial^2 b}{\partial z^2} - \frac{\partial^4 b}{\partial z^4} \qquad \text{for } \frac{\partial b}{\partial z} < 0. \tag{29b}$$

The nonlinearity of this system is hidden in the specification of the convecting and interfacial zones.

The system of equations (29) has been integrated numerically. A pseudospectral model was initiated by a uniform buoyancy gradient slightly perturbed by the linearly fastest-growing unstable mode of (29*a*). The height of the computational domain was $L_z = 71$, which is equivalent to eight fastest growing wavelengths, and $K_c/|K_f| = 10^3$. The first stage in evolution of the buoyancy profile (figure 4*a*) is characterized by the monotonic growth of the unstable normal mode. By $t = 20$ (figure 4*b*), the amplitude of the perturbation becomes sufficient to create density inversions, where the convective dynamics are represented by (29*b*). Since the diffusivity in such regions is extremely high, buoyancy in layers becomes nearly homogeneous. Figures 4(*c*)–4(*f*) illustrate the evolution of the newly formed staircase in time: steps start to merge continuously, and the coarsening continues until there is only one interface left. Figure 5 plots the buoyancy gradient $g = b_z$ as a function of time and z. While this and the previous (figures 2 and 3) experiments are both characterized by the continuous coarsening of a staircase, there is a principal difference in the mechanics of merging events. Unlike in the Balmorth *et al.* (1998) model, layers in figures 4 and 5 merge when the

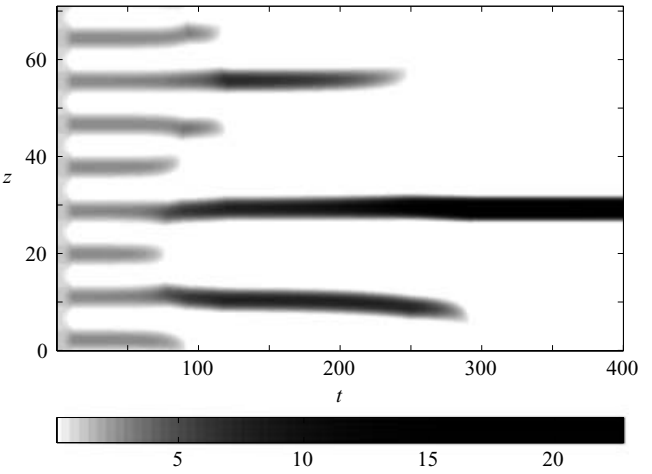

FIGURE 5. Space–time diagram of the buoyancy gradient for the experiment in figure 4. Unlike the calculation in figure 3, layers merge when the relatively strong interfaces grow further at the expense of weaker interfaces which gradually decay and eventually disappear (the B-merger scenario).

relatively weak interfaces decay and eventually disappear without moving vertically. A number of experiments were performed with different parameters for the problem. All of them indicate that the B-merger – erosion of weak interfaces – is a generic property of the upgradient flux model in (29), the property which we rationalize in the next section using the merging theorem.

4. Rationalization of the numerical results

Now we examine whether the behaviour observed in the numerical experiments (§ 3) is consistent with the predictions of our theoretical model in § 2.

4.1. *Mechanically forced stratified turbulence: H-merger*

Numerical solutions of the Balmforth *et al.* (1998) model equations revealed that the formation of a staircase is followed by a series of H-mergers. To explain this numerical result, we compute the growth rates of the B- and H-instabilities in (23). The asymptotic ($\tilde{H} \to \infty$) expression for the steady one-step flux $\tilde{F}$ is given by (A18) in Appendix A. Recalling that $\tilde{B} = \bar{g}\tilde{H}$, we rewrite the λ_B-equation in (23) as

$$\lambda_B = -\frac{4}{H^2} \left. \frac{\partial \tilde{F}}{\partial \bar{g}} \right|_{\tilde{H}=const}. \tag{30}$$

Substituting (A18) in (30) yields:

$$\left.\begin{aligned} \lambda_B &= \frac{4}{H} \frac{\alpha_1^{1.5} g_{max}}{\gamma(g_{max} - g_{min})} \exp(-2a_1 H) \quad \text{for } \bar{g} < g_0, \\ \lambda_B &= \frac{4}{H} \frac{\alpha_2^{1.5} g_{min}}{\gamma(g_{max} - g_{min})} \exp(-2a_2 H) \quad \text{for } \bar{g} > g_0, \end{aligned}\right\} \tag{31}$$

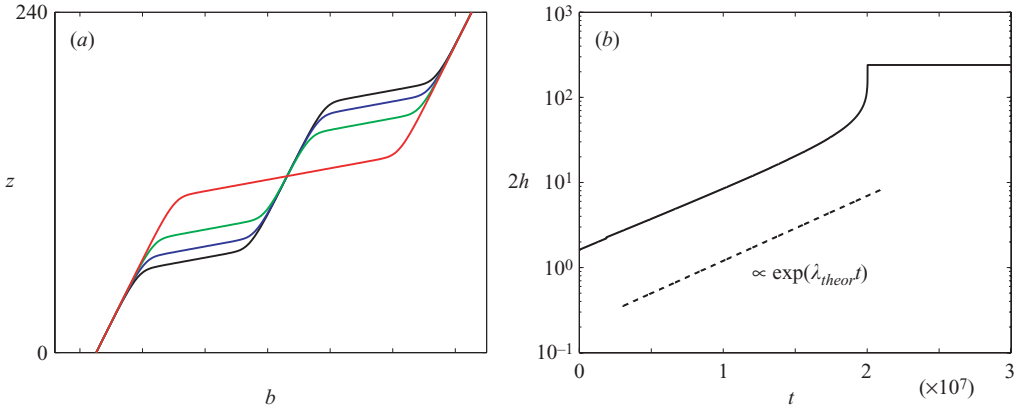

FIGURE 6. Evolution of the buoyancy profile in the numerical experiment with the periodic 'two-step' solution of the Balmforth *et al.* (1998) model eqations. (*a*) The buoyancy distribution at $t=0$, $t=1.8\times10^7$, $t=2\times10^7$ and $t=3\times10^7$ is indicated by the black, blue, green and red curves, respectively. The initial buoyancy profile consists of two nearly identical steps. In time, the thickness of one of the steps continuously decreases and, eventually, the system evolves to a steady one-step configuration. (*b*) The difference in step heights of the experiment in (*a*) is plotted in logarithmic coordinates as a function of time (solid line). The theoretical growth predicted by (36) is indicated by the dashed line.

and the values of constants in (31) are given in (A21)–(A24) in Appendix A. Similarly, the λ_H-equation in (23) is rewritten, making use of (A18) and (A27), as

$$\lambda_H = \frac{4\left.\dfrac{\partial\tilde{F}}{\partial\tilde{H}}\right|_{\tilde{B}=const}}{B-\dfrac{\Delta B_L}{2}-\dfrac{H}{2}\dfrac{\partial\Delta B_L}{\partial\tilde{H}}} \approx \frac{4\left(\left.\dfrac{\partial\tilde{F}}{\partial\tilde{H}}\right|_{\bar{g}=const}-\dfrac{\bar{g}}{H}\left.\dfrac{\partial\tilde{F}}{\partial\bar{g}}\right|_{\tilde{H}=const}\right)}{H(\bar{g}-g_{min})}. \tag{32}$$

When the asymptotic expression for the one-step flux (A18) is substituted into (32), we arrive at the explicit expression for λ_H:

$$\left.\begin{aligned}\lambda_H &= \frac{4}{H(\bar{g}-g_{min})}\frac{\alpha_1^{1.5}g_{max}g_{min}}{\gamma(g_{max}-g_{min})}\exp(-2a_1H) \quad \text{for } \bar{g}<g_0,\\ \lambda_H &= \frac{4}{H(\bar{g}-g_{min})}\frac{\alpha_2^{1.5}g_{max}g_{min}}{\gamma(g_{max}-g_{min})}\exp(-2a_2H) \quad \text{for } \bar{g}>g_0.\end{aligned}\right\} \tag{33}$$

Since the growth rates in (31) and (33) are always positive, the staircase supports both H- and B-instabilities. To explain the apparent (see figure 3) preference for the H-mergers in the numerical simulations, we compare λ_H and λ_B:

$$\left.\begin{aligned}\frac{\lambda_B}{\lambda_H} &= \frac{\bar{g}-g_{min}}{g_{min}} < \frac{g_0-g_{min}}{g_{min}} = 0.49 \quad \text{for } \bar{g}<g_0,\\ \frac{\lambda_B}{\lambda_H} &= \frac{\bar{g}-g_{min}}{g_{max}} < \frac{g_{high}-g_{min}}{g_{min}} = 0.18 \quad \text{for } \bar{g}>g_0.\end{aligned}\right\} \tag{34}$$

Thus, H-instability grows faster than B-instability, and therefore unbiased initial conditions are likely to result in a series of H-mergers.

To validate our theoretical model on a quantitative level, we also performed a more controlled experiment using a 'two-step' structure constructed as follows. First,

we numerically computed the steady one-step solution whose height is $\tilde{H}=120$ and $\tilde{B}=\bar{g}\tilde{H}=3$, which was then combined with another identical step. A small-amplitude random noise was added to expedite the instability and the result was integrated in time numerically. Figure 6(*a*) shows the evolution of this system to a new one-step steady state, twice as large as the original; the two steps H-merged. In figure 6(*b*), we plot the difference in heights ($2h$) of the two steps in logarithmic coordinates as a function of time and compare its growth with the prediction of the merging theorem. The theoretical growth rate can be, in principle, evaluated using our asymptotic ($H\to\infty$) expression in (33). However, this asymptotic estimate is not sufficiently accurate for the relatively thin layers in figure 6. Therefore, the theoretical growth rate has been computed directly from (23), which requires knowing the derivative of the one-step flux ($\tilde{F}$) with respect to the step height. This quantity was estimated by performing two numerical experiments in which the height of the one-step structure ($\tilde{H}$) was varied, whereas $\tilde{B}$ was kept constant. The resulting fluxes equilibrated at the level of

$$\left.\begin{aligned}\tilde{F}(\tilde{H}_1)&=7.47070\times10^{-3},\quad \tilde{H}_1=124,\\ \tilde{F}(\tilde{H}_2)&=7.47013\times10^{-3},\quad \tilde{H}_2=116.\end{aligned}\right\}\tag{35}$$

Using these fluxes, we evaluate $\partial\tilde{F}/\partial\tilde{H}$ and thus independently estimate the linear growth rate of the merging instability in figure 6:

$$\lambda_H=\frac{4\left.\dfrac{\partial\tilde{F}}{\partial\tilde{H}}\right|_{\substack{\tilde{H}=H\\ \tilde{B}=B}}}{H(\bar{g}-g_{min})}\approx 1.76\times10^{-7}.\tag{36}$$

The theoretical prediction (36) is plotted (dashed line) along with the numerical result in figure 6(*b*), and their apparent agreement supports our theoretical model of merging in § 2. Another notable feature of the experiment in figure 6 is related to the subcritical character of merging instability; the finite-amplitude effects tend to further accelerate the merging process. Thus, once initiated, the instability does not saturate at finite level, but grows until the complete merger of the adjacent layers.

4.2. *Mechanically forced stratified turbulence: B-merger*

Equations (31) and (33) indicate that the Balmforth *et al.* (1998) model is affected by both B- and H-instabilities and the reason for the apparent preference of the H-merger dynamics in figures 2, 3 and 6 is related to its higher growth rate (λ_H). It is of interest, however, to determine whether the B-merger dynamics can be realized for some specific initial conditions. Therefore, our next experiment was initiated by a two-step structure with identical step heights ($H=150$), but with slightly different (by 3%) buoyancy variations across the steps. Since (34) suggests that the growth rates of H- and B-instabilites are not drastically different for $\bar{g}\to g_0^-$, we used $\bar{g}=0.016$. The computational domain $L_z=2H=300$ was resolved by $N=128$ elements and the resulting evolutionary pattern of buoyancy gradient is shown in figure 7. As in our previous two-step calculation (figure 5), this structure gradually evolved to a one-step configuration. This time, however, the transition to the final state followed the B-merger scenario – the interfaces did not visibly move throughout the experiment, but a weaker interface gradually eroded and eventually disappeared.†

† A reviewer pointed out that this B-merger experiment can be considered as a counterexample to the conventional vision of coarsening in systems of the Cahn–Hilliard type. Dynamics of such

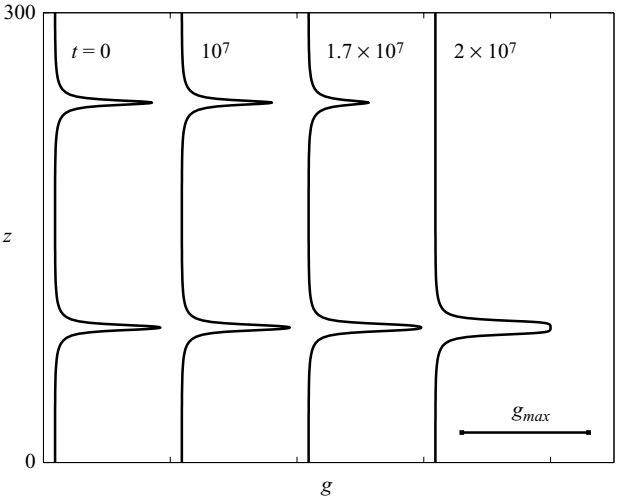

FIGURE 7. Time evolution of the buoyancy gradient in the two-step experiment with the Balmforth *et al.* (1998) model. Initially, two steps are of equal height, but have slightly different buoyancy variations. In time, the layers B-merged to form a single step. This calculation illustrates the significance of the initial condition for selection of the merging pattern in models supporting both B- and H-instabilities.

4.3. *Upgradient flux model*

Finally, the merging theorem is applied to the upgradient flux model discussed in § 3.2. The explicit expression (B10) for the one-step buoyancy flux ($\tilde{F}$) is derived in Appendix B. Substituting (B10) into (23) yields

$$\lambda_B = -\frac{4}{H}\frac{\partial \tilde{F}}{\partial \tilde{B}}\bigg|_{\substack{\tilde{H}=H \\ \tilde{B}=B}} = \frac{2}{\pi H} > 0, \tag{37}$$

which proves that the system of layers in the negative buoyancy flux model is always unstable with respect to the B-merging instability. On the other hand, the growth rate of H-merging instability in (23) is exactly zero, since the one-step buoyancy flux $\tilde{F}$ is independent of $\tilde{H}$. These findings explain the evolution of the numerical staircase in figures 4 and 5, undergoing a series of B-mergers until step size reaches the maximum scale resolved by the computational domain.

To be more quantitative in comparing the numerical results with theoretical predictions, we performed a numerical experiment with the 'two-step' structure. The steady-state solution in figure 4(f) was combined with another identical step and a small-amplitude random noise was added to expedite the instability. The result was integrated in time numerically. Figure 8(a) shows the evolution of this system which leads to a new one-step steady state, twice as large as the original. As expected,

models is generally discussed in terms of the metastable equilibrium solutions which evolve by following, in our notation, the H-merger scenario (e.g. Legras, Frisch & Villone 1999).

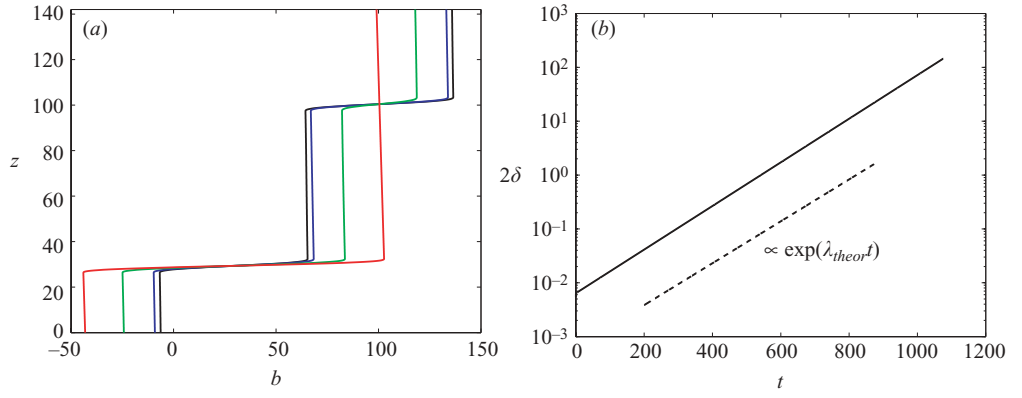

FIGURE 8. Evolution of the buoyancy profile in the numerical experiment with the periodic 'two-step' solution of the upgradient flux model. (*a*) The buoyancy distribution at $t = 0$, $t = 800$, $t = 1000$ and $t = 1500$ is indicated by the black, blue, green and red curves, respectively. The initial buoyancy profile consists of two nearly identical steps. In time, the buoyancy jump across the upper (lower) interface continuously decreases (increases). The upper interface is eventually eliminated and the system evolves to a steady one-step configuration. (*b*) The difference in buoyancy jumps across the two interfaces in (*a*) is used as a measure of strength of the B-merging perturbation and is plotted in logarithmic coordinates as a function of time (solid line). Also plotted (dashed line) is the theoretical prediction for the exponential growth from (37).

the merger of the two steps followed the B-merger scenario. In figure 8(*b*), we plot (solid line) the difference in buoyancy variation across the two steps (2δ) in logarithmic coordinates as a function of time. Also plotted (dashed line) is the theoretical prediction for the growth rate of the disturbance from (37). The apparent agreement between the theoretical and numerical results lends credence to the merging theorem in § 2. A small (∼3%) error of the theoretical estimate is attributed to the finite thickness of high-gradient interfaces, which has not been taken into account by the merging theorem.

The success of our theory also implies that the instantaneous fluxes in merging layers are well represented by the steady-state one-step fluxes – one of the critical assumptions of the merging theorem. This feature is readily understood by comparing the time scale of flux adjustment in one-step solutions to changes in H or B with the time scale of merging instability. The former is controlled by the speed of adjustment of thin high-gradient interfaces:

$$t_{adj} \sim \Delta b \ll \frac{\partial \bar{b}}{\partial z} H = H, \tag{38}$$

whereas the merging time scale can be estimated from the growth rate of the B-instability in (37):

$$t_B \sim \frac{1}{\lambda_B} = \frac{\pi H}{2}. \tag{39}$$

The inequality $t_B \gg t_{adj}$ justifies the use of the one-step steady-state flux law in Appendix B for the description of the slowly evolving system of merging layers.

5. Discussion and conclusions

Layers of relatively mixed water separated by the high-gradient interfaces are frequently observed in stratified lakes and in the ocean. Such stepped structures have also been reproduced in laboratory and numerical experiments with stratified turbulent fluids. Spontaneous generation of layers is generally attributed to the instabilities of the equilibrium with uniform stratification, and similar processes are known to occur in many other physical systems (e.g. theory of phase transitions, Cahn & Hilliard 1958). After their formation, layers typically undergo a series of merging events which greatly increase their average height. This study attempts to explain the dynamics of coarsening and to develop a sufficiently general technique for predicting, from given buoyancy flux laws, the evolutionary pattern of layers. We identify two principal mechanisms of coarsening: the B-merger, involving the growth of relatively strong interfaces at the expense of weaker interfaces, which gradually decay and eventually disappear, and H-merger, characterized by the vertical drift and collision of the adjacent interfaces. This evolutionary behaviour is explained by the linear stability analysis for a series of identical layers and interfaces – the merging theorem – which suggests that the two types of merger are manifestations of two distinct modes of instability. The first mode is unstable if the buoyancy flux decreases with the buoyancy variation across the step, and is shown to cause the B-merger, whereas the H-instability occurs when the buoyancy flux increases with the step height.

The merging theorem has been applied to two one-dimensional models of mixing: the model of the mechanically forced turbulence formulated by Balmforth *et al.* (1998), and the upgradient flux model (Merryfield 2000). For the upgradient model we predict – and confirm by numerical simulations – that the staircase is always unstable with respect to B-instability, but does not support the H-mergers. The situation with regard to the Balmforth *et al.* (1998) model is more complicated: both instabilities are always present. However, the growth rate of H-instability exceeds the growth rate of B-instability, which explains the preference for H-mergers in the numerical experiments with unbiased initial conditions. Both types of coarsening have been observed in the laboratory experiments (Park *et al.* 1994).

Although discussion in this paper is focused on prominent staircases, presumably formed by fully developed turbulence, we believe that many aspects of our theory may be qualitatively relevant to less pronounced examples of layered systems. Balmforth & Young (2005), for instance, show that layering may also develop as a result of the nonlinear evolution of laminar mixing flows. The resulting system of gentle layers frequently exhibit coarsening, not unlike that discussed in our study. Direct numerical simulations in Simeonov & Stern (2007) indicate that interactions in a vertically periodic system of lateral intrusions also lead to the binary mergers which increase their vertical scale. It is therefore possible that the upscale transfer of buoyancy variance associated with merging events is a significant source of the fine-scale ($\sim$10 m) variability in the regions of active mixing in the ocean.

Finally, we wish to point out that although in our specific examples (Balmforth *et al.* 1998; Merryfield 2000) the layer merging goes on indefinitely, there is no reason to assume that the endless coarsening is a generic feature of staircases. Existing formulations of the buoyancy flux laws, which typically rely on crude heuristic arguments, are not intended to express the complete quantitative theory of stratified turbulence. Hence, it is likely that advances in our understanding of mixing in stratified fluids will lead to modification of these models. As demonstrated by Radko (2005), taking into account some subtle effects in the formulation of the flux laws

may lead to the appearance of a critical scale of layers beyond which the coarsening is arrested. Thus, we suggest that future effort should be directed towards formulating the physically based mixing models capable of representing the eventual equilibration of staircases. The simple technique for quantifying the layer-merging characteristics that we develop and illustrate herein should prove helpful in this regard.

The author thanks Neal Balmforth, William Merryfield, and reviewers for helpful comments. Support of the National Science Foundation (grant OCE 0547650) is gratefully acknowledged.

Appendix A. The elementary one-step solution for the Balmforth *et al.* (1998) model

To determine how the steady flux ($\tilde{F}$) in the elementary one-step solution of Balmforth *et al.* (1998) equations responds to changes in the buoyancy variation across the step ($\tilde{B}$) and step height ($\tilde{H}$), we adopt their description of the steady states which casts the energy equation (25) in the following form:

$$\tfrac{1}{2}e_b^2 + U(e) = E, \tag{A 1}$$

where

$$U = -\tfrac{1}{3}\psi - \tfrac{1}{6}\ln\left(\frac{\psi-1}{\psi+1}\right) + \tfrac{1}{2}\ln e + \frac{1}{R\tilde{F}^2}\left(\frac{e^2}{2} - \frac{e^3}{3}\right), \quad \psi = \sqrt{1+\frac{4e^3}{\tilde{F}^2}}. \tag{A 2}$$

Equation (A1) is the canonical equation of motion of the nonlinear oscillator, in which buoyancy b plays the role of time, e is the displacement, and U is the potential. The representative pattern of $U(e)$ (figure 9) is characterized by two local maxima: $U_1 = U(e_{min})$ and $U_2 = U(e_{min})$. The pattern of the $e(b)$ relation can be described as a series of periodic nonlinear oscillations of e within a region bounded by these maxima. For a given value of E in (A1), e oscillates in between e_1 and e_2 – two solutions of the equation $U(e) = E$:

$$e_{min} < e_1 \leqslant e \leqslant e_2 < e_{max}. \tag{A 3}$$

Our discussion here is focused on the limit of large layer thickness ($\tilde{H} \to \infty$) and finite overall buoyancy gradient ($\bar{g}$). This limit corresponds to large total buoyancy variation across the step ($\tilde{B} = \bar{g}\tilde{H}$), and also requires large individual buoyancy variations across its low-gradient layer region (ΔB_L) and the high-gradient interface (ΔB_I). The situation in which large variations in buoyancy are accompanied by finite variations in e– in both layers and interfaces – implies that e_b is low in most of the domain. In view of (A1), this requires that:

(i) E and the two maxima of the potential are nearly equal ($U_1 \approx U_2 \approx E$);

(ii) the value of e in the bulk of each layer (interface) is sufficiently close to e_{max} (e_{min}).

Extending the analogy with the motion of a nonlinear oscillator even further, we note that the large-layer-thickness regime corresponds to a long period oscillation of a particle between the two nearly equal maxima of the potential U. If the energy of the particle is sufficiently close to the maxima of U, the particle spends most of time near the potential peaks, whereas the transition between these two regimes is relatively rapid. As discussed in Balmforth *et al.* (1998), the configuration in which $U_1 = U_2$, corresponds to a specific value of the flux (F^*), and therefore fluxes in thick steps are sufficiently close to F^*. However, the merger dynamics is actually controlled by this slight variation of flux – the variation which we analyse next.

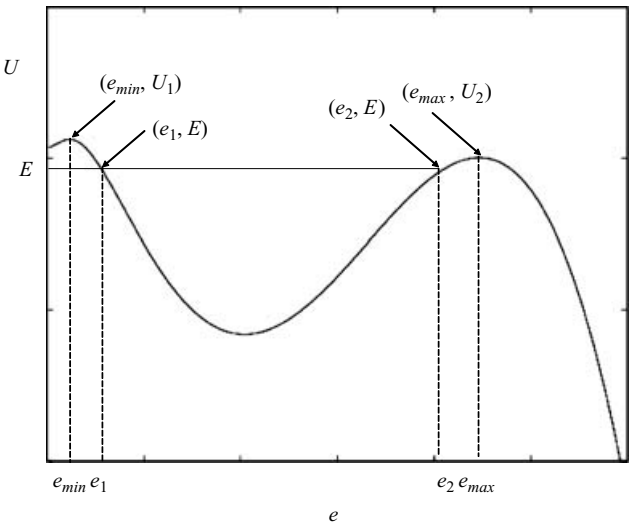

FIGURE 9. Schematic diagram illustrating the asymptotic ($\tilde{H} \to \infty$) analysis of the steady one-step fluxes in the Balmforth *et al.* (1998) model (see the text).

To describe analytically flux in the one-step solution in the limit $\tilde{H} \to \infty$, we focus on the regions of the $U(e)$ relation (see figure 9) in the immediate vicinity of its local maxima – e_{max} and e_{min}. Retaining the leading-order terms in the Taylor expansion of the potential, we approximate U there as follows:

$$\left.\begin{aligned} U(e) &\approx U_1 - \alpha_1 \frac{(e - e_{min})^2}{2} \quad \text{for } e \to e_{min}, \\ U(e) &\approx U_2 - \alpha_2 \frac{(e - e_{max})^2}{2} \quad \text{for } e \to e_{max}, \end{aligned}\right\} \tag{A 4}$$

where $U_{1,2}$, $\alpha_{1,2}$, e_{min}, e_{max} are the constants; their numerical values can be readily estimated from the expression for the potential (A2) for $\tilde{F} = F^*$. Next, consider E which is sufficiently close to U_1 and U_2. The lowest (e_1) and the highest (e_2) values of e, for any given E, can be obtained by requiring that $e_b = 0$ in (A1) and using (A4):

$$E \approx U_1 - \alpha_1 \frac{(e_1 - e_{min})^2}{2}, \quad E \approx U_2 - \alpha_2 \frac{(e_2 - e_{max})^2}{2}. \tag{A 5}$$

The (leading-order) buoyancy variation over the layers and interfaces is determined by rewriting (A1) as

$$\frac{\mathrm{d}b}{\mathrm{d}e} = \frac{1}{\sqrt{2[E - U(e)]}}, \tag{A 6}$$

and then integrating (A6) over the interface:

$$\Delta B_I = \int_{e_1}^{e'} \frac{\mathrm{d}e}{\sqrt{2[E - U(e)]}}, \tag{A 7}$$

where e' is (rather loosely) defined here as a point which is sufficiently close to e_{min}, that the Taylor expansion in (A4) is still applicable, and yet separated from e_{min} much farther than e_1:

$$e_1 - e_{min} \ll e' - e_{min}. \tag{A 8}$$

Using (A4), we approximate the integral in (A7) as

$$\Delta B_I = \int_{e_1}^{e'} \frac{\mathrm{d}e}{\sqrt{\alpha_1[(e-e_{min})^2-(e_1-e_{min})^2]}} = \frac{1}{\sqrt{\alpha_1}} a\cosh\frac{e'-e_{min}}{e_1-e_{min}}. \tag{A 9}$$

Taking (A8) into account further reduces (A9) to

$$\Delta B_I \approx \frac{1}{\sqrt{\alpha_1}}\ln\left(2\frac{e'-e_{min}}{e_1-e_{min}}\right) \approx -\frac{1}{\sqrt{\alpha_1}}\ln(e_1-e_{min}). \tag{A 10}$$

Note that (A10) is, at leading order, independent of e', which confirms our expectation that the buoyancy variation over the interface is largely determined by the pattern of the potential $U(e)$ in the immediate vicinity of e_{min}. Similarly, we estimate the buoyancy variation over the low-gradient layer as

$$\Delta B_L \approx -\frac{1}{\sqrt{\alpha_2}}\ln(e_{max}-e_2). \tag{A 11}$$

Equations (A10) and (A11) are used to estimate the layer and interface thicknesses:

$$H_L = \frac{\Delta B_L}{g_{max}}, \quad H_I = \frac{\Delta B_I}{g_{min}}, \tag{A 12}$$

where g_{min} (g_{max}) are the values of the buoyancy gradient corresponding to e_{max} (e_{min}).

Next, we insist that the sum of the buoyancy variations across the layer and the interface in (A10), (A11) is equal to the total buoyancy variation $\tilde{B}=\bar{g}\tilde{H}$ and, similarly, the sum of their thicknesses in (A12) is equal to the total step height $\tilde{H}$:

$$\Delta B_L + \Delta B_I = \tilde{B}, \quad H_L + H_I = \tilde{H}. \tag{A 13}$$

Drawing together (A10)–(A13), we arrive at

$$\left.\begin{aligned} a_1 &= \sqrt{\alpha_1}g_{max}\frac{\bar{g}-g_{min}}{g_{max}-g_{min}} \quad \text{where } a_1 = -\frac{\ln(e_1-e_{min})}{\tilde{H}}, \\ a_2 &= \sqrt{\alpha_2}g_{min}\frac{g_{max}-\bar{g}}{g_{max}-g_{min}} \quad \text{where } a_2 = -\frac{\ln(e_{max}-e_2)}{\tilde{H}}. \end{aligned}\right\} \tag{A 14}$$

The final condition, required to close the problem and determine $\tilde{F}$ as a function $\tilde{B}$ and $\tilde{H}$, comes from the relation between $\Delta U = U_1 - U_2$ and $\tilde{F}$. Since there is a specific flux value $\tilde{F}=F^*$ for which the two maxima of the potential are exactly equal ($U_2=U_1$), and since $\tilde{F}$ is close to F^* for $\tilde{H}\to\infty$, the leading-order Taylor expansion of $\Delta U(\tilde{F})$ yields

$$\Delta U = U_1 - U_2 \approx \gamma(\tilde{F}-F^*). \tag{A 15}$$

Substitution of U_1 and U_2 from (A5) into (A15) results in

$$\alpha_1\frac{(e_1-e_{min})^2}{2} - \alpha_2\frac{(e_2-e_{min})^2}{2} = \gamma(\tilde{F}-F^*), \tag{A 16}$$

which we rewrite in terms of $a_{1,2}$ in (A14) as follows:

$$\alpha_1\exp(-2a_1\tilde{H}) - \alpha_2\exp(-2a_2\tilde{H}) = 2\gamma(\tilde{F}-F^*). \tag{A 17}$$

In the limit $\tilde{H}\to\infty$, this expression further simplifies to

$$\left.\begin{aligned} \alpha_1\exp(-2a_1\tilde{H}) &= 2\gamma(\tilde{F}-F^*) \quad \text{for } a_1 < a_2, \\ -\alpha_2\exp(-2a_2\tilde{H}) &= 2\gamma(\tilde{F}-F^*) \quad \text{for } a_1 > a_2. \end{aligned}\right\} \tag{A 18}$$

Equation (A14) indicates that a_1 (a_2) is an increasing (decreasing) function of $\bar{g}$, and therefore, for fixed $\tilde{H}$, the buoyancy flux $\tilde{F}$ decreases with $\tilde{B}$. As we discuss in § 2, this feature implies that the system of identical layers in the Balmforth *et al.* (1998) model is always unstable with respect to B-instability, and therefore merging events go on indefinitely. The analysis in § 4 indicates that the system is unstable with respect to H-instability as well. Condition $a_1 > a_2$ ($a_1 < a_2$) in (A18) corresponds to a sufficiently large (small) overall buoyancy gradient $\bar{g} > g_0$ ($\bar{g} < g_0$). The value of buoyancy that separates these two regimes is computed by requiring $a_1 = a_2$ in (A14):

$$g_0 = \frac{(\sqrt{\alpha_1} + \sqrt{\alpha_2}) g_{min} g_{max}}{\sqrt{\alpha_1} g_{max} + \sqrt{\alpha_2} g_{min}}. \tag{A 19}$$

For a more quantitative discussion of merging instabilities, we now calibrate the one-step flux law predicted by our asymptotic ($\tilde{H} \to \infty$) model. The configuration for which the two maxima of the potential are equal occurs for $\tilde{F} = F^* = 0.00747$ (see Balmforth *et al.* 1998). From (A2), we calculate the location of the two maxima at $\tilde{F} = F^*$:

$$e_{min} = 0.022,\ e_{max} = 0.449, \tag{A 20}$$

which corresponds to the buoyancy gradients of

$$g_{min} = 0.0113,\ g_{max} = 0.1342; \tag{A 21}$$

the coefficients of the Taylor expansion in (A4) are:

$$\alpha_1 = -\left.\frac{\partial^2 U}{\partial e^2}\right|_{e=e_{min}} = 209,\ \alpha_2 = -\left.\frac{\partial^2 U}{\partial e^2}\right|_{e=e_{max}} = 66; \tag{A 22}$$

and g_0 in (A19) is estimated using (A20)–(A22):

$$g_0 = 0.0168. \tag{A 23}$$

Likewise, we use (A2) to calibrate the coefficient γ in (A15):

$$\gamma = \frac{\partial \Delta U}{\partial \tilde{F}} = 3.24 \times 10^3, \tag{A 24}$$

which makes our expression for the buoyancy flux in (A17) explicit.

For completeness, we also quantify the dependence of ΔB_L – the variation of buoyancy in the interior of layers in (23) – on $\tilde{H}$ and $\tilde{B}$. For that, we make use of the observation (Balmforth *et al.* 1998) that the buoyancy gradient in the interior of layers (g_L) satisfies the 'equilibrium flux-gradient relation' – a unique relation between g_L and $\tilde{F}$– which we linearly approximate in the vicinity of F^*as

$$g_L \approx g_{min} + \omega(\tilde{F} - F^*). \tag{A 25}$$

Equation (A25) makes it possible to evaluate how the buoyancy variation across the layer responds to changes in $\tilde{H}$ – the information required to compute the growth rate of H-merging instability in (23):

$$\frac{\partial \Delta B_L}{\partial \tilde{H}} \approx \frac{\partial (g_L \tilde{H})}{\partial \tilde{H}} = g_{min} + \omega \frac{\partial \tilde{F}}{\partial \tilde{H}}. \tag{A 26}$$

Noting that $\partial \tilde{F}/\partial \tilde{H}$ becomes exponentially small for $\tilde{H} \to \infty$, (A26) is further reduced to

$$\frac{\partial \Delta B_L}{\partial \tilde{H}} \approx g_{min}. \tag{A 27}$$

Appendix B. The elementary one-step solution for the upgradient flux model

Consider a steady one-step solution of the upgradient flux model (29), exemplified by the final state of the numerical experiment in figure 4(f). The one-step solution consists of a thin high-gradient interface bounded by much thicker, almost homogeneous convective layers. $\tilde{B}$ is the overall buoyancy variation across the step and $\tilde{H}$ is the step height. Without loss of generality, the origin of the coordinate system is placed exactly at the centre of the interface. Thus the interface, where buoyancy increases with z, occupies a finite interval $-l < z < l$, and the buoyancy gradient vanishes at its endpoints:

$$b_z(-l) = b_z(l) = 0. \tag{B 1}$$

The constant downward vertical buoyancy flux in the interface is given by

$$\tilde{F} = -\frac{\partial b}{\partial z} - \frac{\partial^3 b}{\partial z^3} \quad \text{for } -l < z < l, \tag{B 2}$$

and the buoyancy distribution in the interface satisfies the steady form of (29a):

$$\frac{\partial^2 b}{\partial z^2} + \frac{\partial^4 b}{\partial z^4} = 0, \tag{B 3}$$

whose general solution is given by

$$b = C_1 \sin(z) + C_2 \cos(z) + C_3 z + C_4. \tag{B 4}$$

Boundary conditions (B1) requires that $C_2 = 0$, and therefore

$$b_z = C_1 \cos(z) + C_3. \tag{B 5}$$

At $z = \pm l$, the interface smoothly merges with the nearly homogeneous mixed layers, and therefore we also insist on the continuity of the second derivative of buoyancy:

$$b_{zz}(-l) = b_{zz}(l) = 0, \tag{B 6}$$

which implies that

$$\sin(l) = 0 \;\rightarrow\; l = \pi n,\; n = 1, 2, \ldots . \tag{B 7}$$

Numerical simulations indicate that the gradient in the interface monotonically increases towards the centre of the interface, which corresponds to $n = 1$ in (B7), and therefore

$$l = \pi. \tag{B 8}$$

Drawing together (B1), (B5) and (B8) yields $C_3 = C_1$.

Since the convecting layer is nearly homogeneous, the total buoyancy variation across the step ($\tilde{B}$) is dominated by the contribution from the interface:

$$\tilde{B} \approx b(l) - b(-l) = 2C_3 l = 2\pi C_3. \tag{B 9}$$

The vertical buoyancy flux (B2) is calculated from (B5):

$$\tilde{F} = -C_3 = -\frac{\tilde{B}}{2\pi}. \tag{B 10}$$

Equation (B10) indicates that the buoyancy flux in steady one-step solutions decreases with $\tilde{B}$ and is largely independent of $\tilde{H}$. As we discuss in § 2, this feature is critical for the dynamics of merger events in a staircase – it implies that the system of identical layers is always unstable with respect to B-instability, but stable with respect to

H-instability. Thus, B-merging events in the upgradient flux model are expected go on indefinitely.

REFERENCES

Balmforth, N. J. & Young, Y.-N. 2002 Stratified Kolmogorov flow. *J. Fluid Mech.* **450**, 131–167.

Balmforth, N. J. & Young, Y.-N. 2005 Stratified Kolmogorov flow. Part 2. *J. Fluid Mech.* **528**, 23–42.

Balmforth, N. J., Llewellyn Smith, S. G. & Young, W. R. 1998 Dynamics of interfaces and layers in a stratified turbulent fluid. *J. Fluid Mech.* **355**, 329–358.

Bates, P. & Xun, J. 1995 Metastable patterns for the Cahn Hilliard equation, Part II. *J. Diffl Eqns* **117**, 165–216.

Cahn, J. W. & Hilliard, J. E. 1958 Free energy of a nonuniform system. I. Interfacial free energy. *J. Chem. Phys.* **28**, 258–267.

Chapman, C. & Proctor, M. 1980 Nonlinear Rayleigh–Bénard convection with poorly conducting boundaries. *J. Fluid Mech.* **101**, 759–782.

Holford, J. M. & Linden, P. F. 1999 Turbulent mixing in a stratified fluid. *Dyn. Atmos. Oceans* **30**, 173–198.

Huppert, H. E. 1971 On the stability of a series of double-diffusive layers. *Deep-Sea Res.* **18**, 1005–1021.

Kelley, D. E., Fernando, H. J. S., Gargett, A. E., Tanny, J. & Ozsoy, E. 2003 The diffusive regime of double-diffusive convection. *Prog. Oceanogr.* **56**, 461–481.

Legras, B., Frisch, U. & Villone, B. 1999 Dispersive stabilization of the inverse cascade for the Kolmogorov flow. *Phys. Rev. Lett.* **82**, 4440–4443.

Manfroi, A. & Young, W. 1999 Slow evolution of zonal jets on the beta-plane, *J. Atmos. Sci.* **56**, 784–800.

Merryfield, W. J. 2000 Origin of thermohaline staircases. *J. Phys. Oceanogr.* **30**, 1046–1068.

Meshalkin, L. & Sinai, Y. 1961 Investigation of the stability of a stationary solution of a system of equations for the plane movement of an incompressible viscous fluid. *Z. Angew. Math. Mech.* **25**, 1700–1705.

Panetta, R. L. 1993 Zonal jets in wide baroclinically unstable regions: persistence and scale selection. *J. Atmos. Sci.* **50**, 2073–2106.

Park, Y.-G., Whitehead, J. A. & Gnanadeskian, A. 1994 Turbulent mixing in stratified fluids: layer formation and energetics. *J. Fluid Mech.* **279**, 279–311.

Phillips, O. M. 1972 Turbulence in a strongly stratified fluid: is it unstable? *Deep-Sea Res.* **19**, 79–81.

Posmentier, E. S. 1977 The generation of salinity finestructure by vertical diffusion. *J. Phys. Oceanogr.* **7**, 298–300.

Radko, T. 2003 A mechanism for layer formation in a double-diffusive fluid. *J. Fluid Mech.* **497**, 365–380.

Radko, T. 2005 What determines the thickness of layers in a thermohaline staircase? *J. Fluid Mech.* **523**, 79–98.

Rhines, P. 1975 Waves and turbulence on a beta-plane. *J. Fluid Mech.* **69**, 417–443.

Ruddick, B. R., McDougall, T. J. & Turner, J. S. 1989 The formation of layers in a uniformly stirred density gradient. *Deep-Sea Res.* **36**, 597–609.

Schmitt, R. W. 1994 Double diffusion in oceanography. *Annu. Rev. Fluid Mech.* **26**, 255–285.

Schmitt, R. W. 2003 Observational and laboratory insights into salt finger convection. *Prog. Oceanogr.* **56**, 419–433.

Simeonov, J. & Stern, M. E. 2007 Equilibration of two-dimensional double diffusive intrusions. *J. Phys. Oceanogr.* (in press).

Simpson, J. H. & Woods, J. D. 1970 Temperature microstructure in a freshwater thermocline. *Nature* **226**, 832–834.

Whitham, G. B. 1974 *Linear and Nonlinear Waves*. John Wiley.

Zodiatis, G. & Gasparini, G. P. 1996 Thermohaline staircase formations in the Tyrrhenian Sea. *Deep-Sea Res.* **43**, 665–678.